GLACIAL-INTERGLACIAL CLIMATE CONTROLS ON SEDIMENT SUPPLY

ALONG THE SOUTHERN ARGENTINE MARGIN

By

TIMOTHY GARY SHAMUS

A thesis submitted to the

School of Graduate Studies

Rutgers, The State University of New Jersey

In partial fulfillment of the requirements

For the degree of

Master of Science

Graduate Program in Earth and Planetary Sciences

Written under the direction of

James D. Wright

And approved by

New Brunswick, New Jersey

October, 2022

ABSTRACT OF THE THESIS

Glacial-interglacial climate controls on sediment supply along the southern Argentine margin
By TIMOTHY GARY SHAMUS

Thesis Director:
James D. Wright

The TN372-1909 Research Cruise sailed along the southern Argentine margin September through October 2019. The Piedra Buena terrace is a constructional terrace between 2200 and 2800 m water depth. A south to north transect of cores was collected to study changes along this terrace. Multi-sensor core logger (MSCL) data profiles of magnetic susceptibility (MS) and density show similarities to other jumbo piston cores (JPCs) that were taken along the Piedra Buena terrace. Core 27 GC was collected from the mid-point of the transect and chosen for initial analysis. Five Lithostratigraphic Units were identified in Core 27 GC that consist of alternating layers of biogenic carbonate oozes and quartz-glauconite sands. Starting from the top, Lithostratigraphic Units I (0-25cm), III (45-165 cm), and V (255-360cm) are identified by high biogenic $CaCO_3$, low MS and density, and light color. The coarse fractions of these units have abundant planktonic foraminifera with minor abundances of radiolaria and diatoms. The terrigenous components of these units consists of quartz and glauconite sands. Lithostratigraphic Units II (25-45 cm) and IV (165-255cm) are characterized by terrigenous sediments and glauconite, high MS and density, and a dark color. Quartz and glauconite dominate the sediments deposited in Lithostratigraphic Units II and IV with minor contributions of radiolaria and diatoms. Planktonic foraminifera were absent in Units II and IV. Stable isotopes were performed on *Neogloboquadrina pachyderma* (s) showing low $\delta^{18}O$ values for Units I and V, intermediate values for Unit III and high values going into II and IV

where planktonic foraminifera became absent. Therefore, the first-order control on depositional facies is sea level changes driven by glacial-interglacial cycles. The presence of radiolarians and diatoms in Units II and IV indicate that surface water hydrography also influenced the composition of the sediments with biosiliceous fauna and flora replacing the calcareous counterparts during glacial intervals. The dominance of terrigenous material during the glacial Units II and IV with low to moderate contribution to Units I, III, and V indicates that sediments are trapped on the shelf during sea level highstands and delivered to the canyon system during sea level lowstands. Any age model will need verification from cores to the north. The MSCL profiles were correlated across the Piedra Buena terrace coring transect. The five established lithostratigraphic units can be correlated to all but one core on the terrace. Differences among core logger profile result from large sediment delivery on the terrace related to proximity to submarine canyon systems that transport and redeposit material. Based on correlation of the Lithostratigraphic units, the northernmost cores on Piedra Buena (58 JPC and 43 JPC) record the highest sedimentation rates because of their proximity to large canyon systems. The southernmost core (25 GC) is distinct and provides only tenuous correlation, which may indicate bottom currents are stronger and/or sediment supply was lowest.

AKNOWLEDGEMENTS

I would like to thank my advisors and faculty for their guidance and support throughout the course of my research. To Jim Wright, thank you for holding on to my application despite not having an advisor to work with. Thank you for giving me the opportunity to sail on the cruise that ultimately led to the writing of this thesis. To Rick Mortlock, thank you for working with me in the Stable Isotopes Lab. The discussions we would have in the office and lab really helped the research process. To Ken Miller, thank you for helping me get enrolled here at Rutgers. Thank you for always finding the time to help me work something out or discuss glauconite. To Linda Godfrey, thank you for your guidance in the lab and discussions about different processes we can use to push my research forward. I look forward to working with you as I continue this research. Thank you to Bryan Katchikian for generating the weight % opal data. To everyone else on the faculty, thank you for your help while I adjusted to a field of research and adjusting to being back on campus during the pandemic. To the EPS department, thank you for the TA support. It allowed me to gain valuable teaching experience, while having the opportunity to continue my education and conduct research. I would like to express my thanks to my friends and family for all of their support over these past 3 years. To my parents, thank you for making the sacrifices you made over the years as I worked to achieve my goals. Also thank you for putting up with all of the chaos that I have put you through. Finally, a special thank you to Dr. Claire Condie for motivating me to further my education and providing an immeasurable amount of support throughout my entire academic career.

TABLE OF CONTENTS

LIST OF TABLES

LIST OF FIGURES

1. INTRODUCTION

The sediments deposited along the southern Argentine margin offer an opportunity to explore the interaction among climate, deep-ocean currents, and sediment supply on glacial-interglacial timescales. Knowledge of the sediment sequences that comprise the Argentine margin and the interaction with Southern Ocean water masses is limited. Improving the understanding of paleo- Southern Ocean water masses can lead to improved Pleistocene Ocean circulation and climate reconstructions.

There are very few sites proximal to the origin of Southern Ocean bottom water masses that also interact with the seafloor. The southern Argentine margin is the southernmost margin intersecting the Southern Ocean where these deep-water masses originate, making it an important location to study these water masses as they enter the South Atlantic Ocean. The sediments that accumulate in this region preserve records of the interaction of southern sourced water masses and continental sediments supplied to the margin (Gruetzner et al., 2011), providing an opportunity to study the interplay between sediment supply, bottom water currents and climate, including both sea level and surface water changes, on glacial-interglacial timescales.

Intermediate and deep ocean currents that originate in the Southern Ocean interact with the southern Argentine margin (Reid, 1989; Hernandez-Molina, 2010). These water masses include Antarctic Intermediate water (AAIW), Upper Circumpolar Deepwater (UCDW), Lower Circumpolar Deep Water (LCDW), which flow over the continental slope and continental rise. Antarctic Bottom Water (AABW) flows over the base of the rise and abyssal plain of the Argentine Basin (Figure 1). These currents were generated by the global thermohaline circulation and shaped the seafloor in the Argentine margin and Basin through depositional and erosive episodes (Gruetzner et al., 2010, 2011; Hernandez-Molina et al., 2010).

The constructional and erosive forces along the Argentine margin (Figure 1) produced four terraces found at different depths in a step-like fashion (Hernandez-Molina et al., 2009; Lastras et al., 2011). The terraces developed through the interaction of water masses with the seafloor. Each of the four terraces can be correlated with main interfaces of Antarctic water masses (Hernandez-Molina et al., 2009). The Nagera is the uppermost terrace and forms the continental shelf between 0 and 500 m (Hernandez-Molina et al., 2009). The Perito Moreno terrace ranges from depths of approximately 700 m to 1500 m and coincides with AAIW-UCDW interface at depths of about 1km. The Piedra Buena terrace ranges from depths of 2150 to 3000 m and coincides with the UCDW-LCDW interfaces at depths of about 2.1 and 2.5 km respectively; and the Valentin Feilberg terrace is found in depths greater than 3300 m and coincides with the LCDW-AABW at depths of about 3.5 to 4km (Hernandez-Molina et al., 2009). These terraces are separated by deep channels and moats and form parts of the Argentine contourite drift system (Hernandez-Molina et al., 2009, 2010; Gruetzner et al., 2011; Lastras et al., 2011). Cruise TN372-1909 and this thesis focuses on the Piedra Bena terrace. The uppermost Nagera terrace will become important as a source for terrigenous sediments and the Perito Moreno terrace an important conduit for the sediments supplied to the lower terraces.

The contourite drift system (CDS) described by Hernandez-Molina et al. (2009) displays both erosive and depositional features. Contourite drifts are deposits that result from bottom contour currents (Faugeres et al., 1999). The CDS in the Argentine margin results from topographic intensification of Antarctic-sourced water masses, an increase of downslope sedimentary processes to the north, and local tectonic influences (Hernandez-Molina et al., 2009). Deposition on the CDS started at the Eocene-Oligocene boundary and is believed to be coeval with the opening of the Drake Passage (Hinz et al., 1999). The Piedra Buena and Valentin-Feilberg terraces developed from this constructional system. A change in the CDS morphology to a complex terraced slope without a continental rise due is to the introduction of North Atlantic Deep Water (NADW) into the Southern Hemisphere and the deepening of AABW circulation in the Argentine Basin during the Middle to Late Miocene (Hernandez-Molina et al., 2009). The Argentine CDS is located where water mass circulation of AAIW, UCDW, and LCDW interact with the seafloor topography at depths of less than 1 km to 3.5 km (Piola and Matano, 2001).

Several canyon systems are found along the margin with multiple branches associated with the Patagonian Submarine Canyon System (PSCS) that cut into the terraces of the upper and middle continental slope that trend west to east (Lastras et al., 2011). The northern most canyons are part of the Almirante Brown transverse canyon system which cut into parts of the continental shelf (Lastras et al., 2011). Little information exists on the morphology of the transition between the Perito Moreno and Piedra Buena terraces, but scours and canyons have been imaged in these areas (Lastras et al., 2011).The presence of contourites and canyons in the same location indicate that both down-slope and across-slope processes are present in this part of the margin. Lastras et al., (2011) propose that down-slope processes are more dominant within the Perito Moreno terrace while across-slope processes are more dominant in the Nagera terrace.

1.1 FIELD SITE

Research Cruise TN372-1909 sailed from Montevideo, Uruguay on September 11, 2019 and returned October 31, 2019 aboard the *R/V Thomas G. Thompson* to seismically image and core the southern Argentine margin. The area of study was approximately 45° to 49°S and 51° to 56°W (Figure 2). This section of the Argentine margin is bounded by the Colorado and Malvinas/Falkland fracture zones (Gruetzner et al., 2011).

This study focuses on the Piedra Buena terrace. In the northern part of the study area, a submarine canyon cuts into the Piedra Buena terrace with a WSW-ENE trend (Isola et al., 2021) (Figure 2). This canyon is the continuation of “Canyon # 1” as described by Lastras et al., (2011) and Isola et al., (2021). There exists a west-east trending branch that joins the main canyon in this area as well. (Isola et al., 2021). As discussed later in the thesis, this canyon system is the main canyon system that influences Core 27 GC and other Piedra Buena cores taken in this area.

2. METHODOLOGY

2.1 PIEDRA BUENA CORES

Research Cruise TN372-1909 collected 18 cores from the Piedra Buena terrace using both gravity core (GC) and jumbo piston coring (JPC) systems. Gravity coring (20ft Big Bertha) were collected to test seafloor conditions prior to deploying the jumbo piston corer (40 and 50 ft). To date, the only core sampled on the Piedra Buena terrace is Core 27 GC (46.6382°S, 58.5943°W, 2348 m water depth; Table 1) which recovered 3.6 m of sediment. This coring site was chosen because 3.5 kHz profiles show a transparent layer at the surface with alternating hard reflectors and transparent layers below. Holocene sediments are expected based on a transparent layer just below the seafloor (Figure 3B).

2.2 SHIP-BOARD ANALYSIS METHODOLOGY

All cores from the cruise were analyzed on a multi sensor core logger using the GEOTEK MSCL-S provided by Oregon State University's P-Mag Lab. Details of this methodology will be reported elsewhere (Slowey, Wright et al., in prep). The core logger provided preliminary data on p-wave velocity, resistivity, gamma ray attenuation, magnetic susceptibility, and bulk density. Magnetic susceptibility (MS) and bulk density data were the primary properties used in this study.

2.3 CORE SAMPLING AND PROCESSING

Core 27GC was sampled every 10 cm through the entirety of the core starting at 5-7cm. Sediment samples were dried and weighed. Each sample was then soaked in sodium metaphosphate to disaggregate the clays for approximately 24 hours before washing through a 63 µm wire sieve. A beaker placed beneath the sieve captured the fine fraction. The coarse fraction was collected in filter paper and then dried in an oven. The fines were allowed to settle to allow prior to decanting most of the water and placed into an oven to dry. Once dry, coarse- and fine-fraction weights were divided by the dry mass to determine their relative percent in each sample. Point counts were conducted by identifying 300 random sediment grains within the coarse fraction (Appendix 2). Percentages of each component were calculated and used to classify the sediment lithologies presented below.

2.4 WEIGHT % OPAL METHODOLOGY

To determine the weight % biogenic opal, a wet chemical timed extraction with correction for dissolution of clays was conducted as described in Mortlock and Froelich, (1989). Weight % biogenic opal is reported in Appendix 1.

2.5 PLANKTONIC FORAMINIFERAL STABLE ISOTOPE ANALYSIS

Foraminifera were picked from the >63 µm size fraction because the initial core sampling provided small sample sizes (< 0.5g), yielding a low number of foraminifera. The planktonic foraminiferal species used in this study was *Neogloboquadrina pachyderma* (s) because it was the only taxa found in all samples in which foraminifera were present. Ten to fifteen tests were loaded into vials and dried overnight in an oven. Using a Multiprep peripheral attached to the Optima isotope ratio mass spectrometer, foraminifera samples were reacted in phosphoric acid at 90^{o}C for 13 minutes to release

CO_2. The evolved CO_2 was introduced into the Optima mass spectrometer to determine the $\delta^{18}O$ and $\delta^{13}C$ values of the samples. All samples are reported relative to V-PDB by analyzing an internal reference material (RGF1) that is routinely calibrated to NBS-18, -19, and -20. A typical sample run has 8 calibrated reference material measurements for 24 foraminiferal samples. The long-term 1-sigma precision during analysis was 0.08‰ for $\delta^{18}O$ and 0.005‰ for $\delta^{13}C$. All stable isotope values are reported in Appendix 1.

3. RESULTS

3.1 LITHOLOGIC DESCRIPTION

The description of lithologic units in this thesis is based on the >63µm fraction in each sample. Spot checking of these descriptions was conducted on the <63 µm fraction in several samples and confirmed the coarse fraction based lithologic assignment. The biogenic component in the coarse fraction contained variable amounts of planktonic foraminifera, radiolarians, and diatoms. Glauconite and quartz are the dominant contributors to the terrigenous components with minor contributions of mafic mineral grains. The coarse fraction presented in this thesis include microfossils, indicating a higher coarse fraction than what would have been measured if calculated on carbonate- and biogenic silica- free basis (Figure 3).

Core 27 GC was divided into 5 lithostratigraphic units based on sediment composition with the placement of unit boundaries aided by MS and density variations (Figure 3; Table 2). Lithostratigraphic Unit I is found between the core top and 25 cm and is described as a foraminifera-rich carbonate ooze with variable amounts of glauconite and quartz sand. This unit is characterized by low MS (9-40 x 10^{-8} m^3/kg) and intermediate densities (1.6-1.8 g/cc), low-intermediate weight % opal (~2.5-2.6%), and CF values of approximately 60%. Visually, Unit I is a relatively light-colored section in the core. Components in the >63µm fraction include foraminifera (54%) with a mix of glauconite (24%) and quartz (13%) grains of varying grain sizes. Foraminifera mostly consisted of *N. pachyderma* (s), *Globigerina bulloides,* and *N. pachyderma* (dextral, d) indicating subpolar surface waters (Bé and Hamlin, 1967). Lithic grains were moderately abundant, consisting of glauconite and quartz, potential pyroxenes and amphiboles, and small trace amounts of biotite and muscovite. Glauconite grains increase and foraminifera tests decrease in abundance towards the base of this unit. In addition to planktonic foraminifera other biogenic components include sponge spicules and radiolaria.

Lithostratigraphic Unit II is placed between 25-45 cm and is a glauconitic quartz-rich sand. This unit is easily distinguished for the overlying Unit I by its darker color and is characterized by high MS (25-50 x 10^{-8} m^3/kg) and density (~2.0 g/cc), the lowest weight % opal in the core (<1%), and coarse fraction values of approximately 80%. The > 63µm grains include 47% glauconite, 36% quartz grains, 8% gray metallic grains, 1% black adamantine grains, and the final 8% of diatoms. Terrigenous grains vary in shape from subangular to subrounded and are moderately well sorted. Glauconite grains are pale to dark green, dark-gray to black grains. Both clear and smokey quartz grains are also present. Biogenic material consisted of radiolarians, diatoms, and sponge spicules throughout the entirety of this interval. However, radiolarians were only intermittently present. Figure 4 shows the sediments characteristic of Lithostratigraphic Unit II.

Lithostratigraphic Unit III (45-165 cm) is a foraminiferal carbonate ooze with varying glauconite and quartz content that is characterized by light-colored sediments in the core. Unit III generally has low MS, low density (1.5-1.7 g/cc), intermediate weight % opal values (2.8 to 6.4%), and coarse fraction values generally decrease down section from ~80 to30% (Figure 3). The relative contributions of the components in the >63µm fraction varied downcore. The coarse fraction at the top of Unit III has higher abundances of foraminifera tests with lesser quantities of glauconitic grains, and intermediate weight % opal values. Sample 75-77 cm contains 66% foraminifera tests, 15% glauconite, and 4% quartz. The foraminifera in this interval are dominated by *N. pachyderma* (s) and *G.*

bulloides. At 105-107 cm, the coarse fraction contains 52% foraminifera tests, 20% glauconite, and 10% quartz making up the terrigenous component. Towards the bottom of Unit III, terrigenous grains replace foraminifera as the dominant coarse fraction component and is reflected by MS and density increases. Sample 165-167cm contained 26% foraminifera tests and a terrigenous component that consists of 44% glauconite and 20% quartz. The layer of high weight % opal ranges from approximately 90 to 160 cm. The point count and weight % opal indicates the sediments transition to quartz-glauconite sands with foraminifera above the underlying Lithostratigraphic Unit IV. Figures 4b through 4d contrast the abundance changes in glauconite and foraminifera throughout Lithostratigraphic Unit III.

Lithostratigraphic Unit IV (165-255cm) is a quartz-glauconite sand that is easily recognized as the darkest colored sediments in core 27 GC. Like Unit II, this unit has high MS and high densities (Figure 3). Weight % opal values are lower than those in the overlying unit and coarse fraction values increase to approximately 90% (Figure 3). The relative contributions from different grains in the >63μm fraction varied and is reflected in the MS and density logs. The glauconite grains vary from subangular to subrounded and are moderately sorted. Glauconite grains are pale to dark green, dark-gray to black grains while quartz grains are clear and smokey. Diatoms were significantly more abundant in this unit but trended toward lower values towards the base of this unit.

Unit IV was subdivided based on three peaks visible in the core logger data (175 to 215cm; 215 to 235cm; and 235 to 255cm) that correspond to relative changes in glauconite versus quartz abundances. Subunit IV-a (175 to 215cm) is characterized by 58% glauconite and 32% quartz sands. It has the highest magnetic susceptibility and density in in this lithostratigraphic unit, nearly matching those measured in Lithostratigraphic Unit II.

Subunit IV-b (215 to 235 cm) has the highest quartz component (38%) of all the subunits. It also had the lowest magnetic susceptibility and density of all the glauconitic samples in this core

The third subunit, IV-c (235 to 255 cm), is characterized by contained 52% glauconite and 31% quartz grains. This subinterval has a higher magnetic susceptibility but nearly equal density as the second subinterval. Diatoms (10%) were in a higher abundance towards the top of this interval and decreased with abundance at the bottom of the interval.

The lowermost interval of 27 GC considered Lithostratigraphic Unit V (255-360cm) is a foraminiferal ooze and is the lightest colored unit recovered in the core. This unit is characterized by the lowest MS and density, low-intermediate weight % opal values (1.2-3.1%), and the highest fine component (90-100%) in the entire core. Foraminiferal tests dominate (>90%) the >63μm fraction while and abundances of glauconite and terrigenous sediments (6%) are low (<5% each). Figure 3 shows an example of the sediments that compose Lithostratigraphic Unit V.

3.2 PLANKTONIC $\delta^{18}O$ DATA

Planktonic foraminifera were picked and analyzed for stable isotope values ($\delta^{18}O$ and $\delta^{13}C$). This thesis focuses on the $\delta^{18}O$ record to test the hypothesis that climate, primarily through sea-level changes, controlled the deposition of lithologic units. Countless studies have demonstrated that low $\delta^{18}O$ values are consistent with marine isotope interglacial intervals and higher sea level (Miller et al., 2005). The late Pleistocene $\delta^{18}O$ record also allows for age assignment through correlation to stacked and orbitally tuned records (e.g., Liseicki and Raymo, 2005). Foraminifera were found only in Lithostratigraphic Units I, III, and V, preventing construction of a continuous $\delta^{18}O$ record in Core 27 GC (Figure 5). *N. pachyderma* (s) was the only taxa present in all samples with foraminifera; however, *G. bulloides* and *N. pachyderma* (d) were analyzed when present. All foraminiferal stable isotope values are reported in Appendix 1. The down core stable isotope record presented here is based only on *N. pachyderma* (s). The discussion will focus on the $\delta^{18}O$ record which ranged from 1.8‰ to 3.5‰.

The $\delta^{18}O$ values recorded in Lithostratigraphic Unit I are relatively low (2.2‰) . As noted above, foraminifera are absent in Lithostratigraphic Unit II, where the major biogenic component consisted of radiolarians and diatoms.

Moving down core, the $\delta^{18}O$ record resumes in Lithostratigraphic Unit III at a core depth of 45 cm with higher values (3.1‰) than measured in Unit I. Values remain relatively high until a core depth of 75 cm before increasing to the highest values in the core at 85 to 115 cm ranging between 3.4-3.5‰. At a core depth of 125 cm, values rapidly decrease downcore to the lowest $\delta^{18}O$ values recorded in the core at a depth of 135 cm (1.8‰). Below this level, $\delta^{18}O$ values increase to 2.3‰ at 165 cm below which foraminifera disappear in Lithostratigraphic Unit IV.

The next level with foraminifera was found in the transition from Lithostratigraphic Unit IV to V. At 255 cm, high $\delta^{18}O$ values are recorded (3.3‰) and decrease over the next 20 cm to approximately 2.5‰. From 275 cm to the bottom of Core 27 GC, $\delta^{18}O$ values continue to decrease to approximately 2‰.

3.3 AGE MODEL

The standard in developing age models for Late Pleistocene paleoceanographic studies uses a combination of $\delta^{18}O$ records and radiocarbon analyses if possible. In this study, the small bulk sample sizes make radiocarbon analysis impossible. The absence of planktonic foraminifera in Lithostratigraphic Units II and IV makes the assignment of marine isotope chrons (MIC) more subjective than most studies. However, the $\delta^{18}O$ record generated supplemented by the changes in biogenic components provides a robust age model for testing the primary hypothesis.

Lithostratigraphic Unit I is assigned to MIC 1 based on the $\delta^{18}O$ values and presence of planktonic foraminifera indicating a mix of polar (*N. pachyderma* (s)) and subpolar (*G. bulloides* and *N. pachyderma* (d)), which is similar to modern surface water conditions. The presence of radiolarians and diatoms and absence of foraminifera in Lithostratigraphic Unit II indicates that overlying surface conditions were polar. Other studies in the South Atlantic have documented the northern migration of the polar front by approximately 5° during the last glacial maximum (e.g., Mortlock et al, 1991). Therefore, Lithostratigraphic Unit II is correlated to MIC 2 despite having no $\delta^{18}O$ record in this unit.

The $\delta^{18}O$ appears again in Lithostratigraphic Unit III, recording values that are 0.8 to 1.2‰ higher than those in Unit I. $\delta^{18}O$ records of the open ocean at similar latitudes record a LGM to present $\delta^{18}O$ change close to 1.8 to 2‰. Unit III values are more consistent with MIC 3 and possibly MIC 4. Between 124 and 145 cm, $\delta^{18}O$ values decrease sharply recording the lowest $\delta^{18}O$ values measured in core 27 GC. The core photograph shows a disconformable surface at 130 cm, indicating erosion or nondeposition (Figure 5). Below this disconformable surface, $\delta^{18}O$ values remain low (1.75 to 2.2‰) and are assigned to MIC 5e. The biogenic assemblage is dominated by the same three taxa of planktonic foraminifera as Unit I. The lowermost $\delta^{18}O$ values in Unit III increase downcore to just above Lithostratigraphic Unit IV and are interpreted as Termination II or the MIC 6/5e boundary.

As in Lithostratigraphic Unit II, foraminifera are absent in Lithostratigraphic Unit IV, requiring the consideration of other evidence for correlation. Like Unit II, biosiliceous diatoms and radiolaria confirm the overlying surface waters were polar during the deposition of Unit IV. Therefore, Unit IV is interpreted as MIC 6.

The $\delta^{18}O$ record appears again at 225 cm at the boundary between Lithostratigraphic Units IV and V (Figure 5). These values are relatively high (3.3‰) and are the highest $\delta^{18}O$ values measured in Unit V. The $\delta^{18}O$ values at 275 cm and below are relatively low 2.5 to 1.8‰. The biogenic assemblage in Unit V is dominated by planktonic foraminifera. The lithologic boundary between Units IV and V is interpreted as MIC 7/6 boundary, with the remainder of Unit V assigned to MIC 7.

Refining and constraining age models will require additional $\delta^{18}O$ of planktonic foraminifera data, potential radiocarbon dates, and other biostratigraphic markers such as *Stylatractus universus* and/or *Hemidiscus karstenii* (Charles, 1991) to confirm ages of sediments.

4. DISCUSSION

Several studies have hypothesized that the lithology on the Piedra Buena terrace is controlled by sea level with higher biogenic components accumulated during sea level high stands and higher terrigenous contribution during low stands (Murdmaa et al., 2018). Core 27 GC provides a first-order test for this hypothesize: the light-colored foraminiferal oozes represent deposition during warmer intervals and sea level high stands while dark-colored quartz-glauconite sands were deposited during glacial intervals and sea level low stands. Mechanistically, the hypothesis posits that terrigenous material is stored on the continental shelf (Nagera terrace) during interglacial periods. During glacial intervals, lower sea level allows surface currents to sweep across the shelf, pushing sediments into the canyon system where they are transported downslope.

This hypothesis must eliminate *in situ* formation of glauconite on the Piedra Beuna terrace. The water depth of Core 27 GC (2348 m) indicates that the glauconite was likely transported to the area since glauconite rarely forms in sediments below depths of approximately 1800 m (Cloud, 1955). Glauconite grains were observed to be subangular to subrounded, requiring that some transportation occurred. Ivanova et al., (2020) noticed that glauconite was one of the dominant components in terrigenous sands on Nagera terrace. Murdmaa et al., (2018) suggested that the quartz-glauconite sands of the Nagera were being eroded and transported downslope through the canyons that cut through the Perito Moreno terrace and argued that this transport occurred during sea level falls.

The alternation between planktonic foraminiferal carbonate oozes and quartz-glauconite sands with biogenic components rich in radiolarians and diatoms likely reflect the migration of the polar front to the north. Previous studies (e.g., Mortlock et al., 1991) have shown that sediments north of the polar frontal zone (PFZ) are characterized by lower weight % opal and biosiliceous components and are more abundant in foraminifera. Conversely, sediments south of the PFZ are characterized by higher weight % opal and biosiliceous components and less abundant in foraminifera. The absence of planktonic foraminifera and presence of the biosiliceous components in Lithostratigraphic Units II and IV reflect the shift in the PFZ and not winnowing, dilution, or dissolution.

4.1 CORRELATION OF PIEDRA BUENA CORES

The five facies established in Core 27 GC can be correlated across the entire N-S transect of the Piedra Buena terrace and is described below (Figure 7). Estimated sedimentation rates show a general trend of higher sedimentation in the north with a general decrease in sedimentation rates southward along the terrace (Figure 8 and Appendix 3).

Lithostratigraphic Unit I can be correlated with all of the Piedra Buena cores. Moving north to south, the profile of Lithostratigraphic Unit I appears to be nearly identical, but is slightly expanded in the northernmost cores on the terrace. For example, Lithostratigraphic Unit I is ~ 50 cm thick in the northernmost core, 58 JPC. To the south, almost all of the cores have ~25 cm thickness of Unit I. If Lithostratigraphic Unit I represents the Holocene then sedimentation rates are ~5 cm/kyr for Core 58JPC versus 2.5 cm/kyr for the remaining cores.

Lithostratigraphic Unit II can be correlated among the Piedra Buena cores because of its high MS and density peaks. Like Unit I, Core 58JPC recorded the thickest

(175 cm) and hence, highest sedimentation rates. Cores to the south recorded thicknesses from 45 to 65 cm. Sedimentation rates are difficult to constrain because the age model is imprecise for Unit II; however, if it assumes that the lowest sea levels occurred between 30 and 15 ka, then the rates would be ~12 cm/kyr in the north versus 3 to 4 cm/kyr in the south. Similarly, Lithostratigraphic Unit III recorded the thickest section (200 cm) in the northernmost core compared to more compact Unit III thicknesses ranging from 75 to125 cm to the south. Sedimentation rates are difficult to estimate because of the apparent hiatus found in Core 27GC.

Lithostratigraphic Unit IV consists of the expanded glauconite interval and repeats the pattern of greatest thickness in 58 JPC (325 cm), thinning to 175 cm in 43 JPC while the other cores vary in thickness between 85 and 125 cm. If Unit IV represents all of MIC 6 (180 to 135 ka), then minimum sedimentation rates were ~7 cm/kyr in the north and 1.5 to 2 cm/kyr to the south. Lithostratigraphic Unit V has similar thicknesses at 58 JPC and 43 JPC (290 and 275 cm) whereas, cores in the center of the transect having thicknesses closer to 100 cm with 30JPC being an exception. Further to the south, 57 JPC shows a more compacted Unit V with a thickness of 75 cm, while the southernmost core 25 JPC shows the thinnest Unit V with a thickness of 45 cm. Sedimentation estimates vary from ~10 cm/kyr in north progressively decreasing to 3 to 4 cm/kyr in the center and 1 to 2 cm/kyr in the south.

4.2 INFERRED DIFFERENCES BETWEEN THE CORES

The 5 lithostratigraphic units that were described in 27 GC can be correlated to most of the cores along the Piedra Buena terrace, although there were several differences between cores taken at different latitudes. These differences in MS and density profiles are likely due to the local topographical and bathymetric differences, specifically submarine canyon systems, near these different cores. Figure 2 shows the locations of all the Piedra Buena cores, and nearby canyon systems.

Core 58 JPC, the northern-most core, is situated between two large canyons that are part of the Almirante Brown Submarine Canyon System which is dominated by down-slope transport. Core 58 JPC shows some of the most varied core logger profiles compared to the other Piedra Buena cores. This is likely due to its proximity to these canyons, and its position on the terrace. Since it is the furthest to the north, a different geological province could be supplying different types of terrigenous sediments that are deposited in the area of this core.

Core 43 JPC is situated between two large canyons that are a part of the southernmost Almirante Brown Submarine Canyon System (Lastras et al., 2011). According to Hernandez-Molina et al. (2010), downslope transport is more dominant that the along-slope transport in this area. The southernmost canyon likely supplies this portion of the Piedra Buena terrace with continental and shelf sediments as branches of this canyon interact with the northern most reaches of the Nagera terrace (Hernandez-Molina et al. 2010). This is likely the reason why every lithostratigraphic unit is expanded in this core.

Core 32 JPC is located on the northern side of the canyon system that is interacting with Cores 27 GC, 29 JPC, and 30 JPC. The bottom portions of this core potentially correlate with the core bottoms of 25JPC. The higher sedimentation thought to occur in 32 JPC is due to its close proximity to the northern branch of the submarine canyon system near cores 27 GC, 29 JPC, and 30 JPC. This portion of the canyon system may be transporting greater amounts of shelf material that are being thrown up and out of the canyon during gravity flows.

Cores 27 GC and 29 JPC were taken at the same location. These cores were collected on a contourite drift deposit bounded by two branches of “Canyon 1” described by Lastras et al., (2011). Differences in lithostratigraphic unit thicknesses and MS and density profiles could be due to the type of coring that was used. 27 GC utilized gravity coring while 29 JPC used piston coring, which may have allowed for less compaction of units.

Core 30 JPC is taken nearby Core 27 GC, approximately 10 km to the southwest. The core logger data show very similar profiles to Core 27 GC. Since it is slightly upslope, there may be slightly more deposition occurring, or piston coring could explain the slightly expanded sections and additional peaks.

Continuing southward along the Piedra Buena terrace is Core 57 JPC. This core has a unique upper section compared to the rest of the Piedra Buena cores. The upper 250 cm shows an expanded section that does not correlate well with the core tops of the other cores. It also shows some compacted units (Lithostratigraphic Units III and V) and some expanded units (Lithostratigraphic Units II and IV). The differences in sedimentation are likely due to deposition of material eroded from southern portions of the margin or with the interaction of different submarine canyon systems nearby. Figure 2 shows some canyons in the approximate area of Core 57 JPC that could be bringing additional sediments down slope. The higher resolution topography of the canyon systems is incomplete, and therefore, it is not known if there are larger canyon systems nearby that could be affecting the sedimentation. The lithic grains of Core 57 JPC may also be coming from a different geological province in Patagonia, affecting the core logger profiles. Since it is also to the south, the currents are believed to be stronger and could be eroding some material away.

The southernmost core in the Piedra Buena transect is Core 25 JPC which shows the least amount of similarity to Core 27 GC and the other Piedra Buena cores. Bottom currents are much stronger in this region compared to other parts of the terrace. The Upper Circumpolar Deep Water traveling from the Southern Ocean is appears to be eroding the seafloor and transporting those sediments northward. A large section in Core 25 JPC is uncorrelatable with core logger data showing low MS and density profiles.

5. CONCLUSION

The results of this study show that core 27 GC has 5 lithostratigraphic units that primarily reflect sea level changes due to glacial-interglacial cycles. Intervals of glauconite correspond to glacial events and associated low sea levels. During sea level low stands, there was more down-slope transport from the terraces situated above the Piedra Buena terrace. Specifically, the glauconite was eroded from the Nagera terrace and transported down submarine canyon systems via gravity flows, and redeposited in contourite drift deposits. Intervals of foraminiferal carbonate oozes are believed to be representative of interglacial periods which are associated with higher sea. High sea level and warmer climates trapped the terrigenous sediments on the shelf (Nagera terrace) resulting in a more pelagic style of deposition producing foraminifera-rich carbonate oozes.

Lithostratigraphic Units I, III, and V are correlated to MIC 1, 5e, and 7 respectively. Units II and IV were deposited during the LGM and MIC 6, respectively.

The lithologic facies established in Core 27 GC were correlated along a north to south transect. Cores recovered from the north recorded higher sedimentation due to their proximity to active submarine canyon systems. In the central and southern regions of the transect, sedimentation rates were lower indicating that pelagic sedimentation dominated with small contributions of terrigenous sediments. Cores taken to the south were subjected to stronger currents which likely eroded sediments off the seafloor and transported them northward.

6. REFERENCES

Allison, L. C., Johnson, H. L., Marshall, D. P., & Munday, D. R. (2010). Where do winds drive the Antarctic Circumpolar Current?. *Geophysical Research Letters*, *37*(12).

Bé, A. W., & Hamlin, W. H. (1967). Ecology of Recent planktonic foraminifera: part 3: distribution in the North Atlantic during the summer of 1962. Micropaleontology, 87-106.

Boex, J., Fogwill, C., Harrison, S., Glasser, N. F., Hein, A., Schnabel, C., & Xu, S. (2013). Rapid thinning of the late Pleistocene Patagonian Ice Sheet followed migration of the Southern Westerlies. *Scientific Reports*, *3*(1), 1-6. doi:10.1038/srep02118.

Charles, C. D. (1991). *Late Quaternary ocean chemistry and climate change from an Antarctic deep sea sediment perspective* (Doctoral dissertation, University).

Cloud Jr, P. E. (1955) Physical Limits of Glauconite Formation. *AAPG Bulletin 39(4)*, 484-492.

Faugères, J. C., Stow, D. A., Imbert, P., & Viana, A. (1999). Seismic features diagnostic of contourite drifts. *Marine Geology*, *162*(1), 1-38.

Gruetzner, J., Uenzelmann-Neben, G., & Franke, D. (2010). Seismic images of contourites forming continental slope terraces at the Argentine Margin implications for past changes in thermohaline circulation. *Geotemas (Madrid)*, (11), 59-60.

Gruetzner, J., Uenzelmann-Neben, G., & Franke, D. (2011). Variations in bottom water activity at the southern Argentine margin: indications from a seismic analysis of a continental slope terrace. *Geo-Marine Letters*, *31*(5), 405-417.

Hernández-Molina, F. J., Paterlini, M., Violante, R., Marshall, P., de Isasi, M., Somoza, L., & Rebesco, M. (2009). Contourite depositional system on the Argentine Slope: An exceptional record of the influence of Antarctic water masses. *Geology*, *37*(6), 507-510.

Hernández-Molina, F. J., Paterlini, M., Somoza, L., Violante, R., Arecco, M. A., de Isasi, M., Rebesco, M., Uenzelmann-Neben, G., Neben, S., & Marshall, P. (2010). Giant mounded drifts in the Argentine Continental Margin: Origins, and global implications for the history of thermohaline circulation. *Marine and Petroleum Geology*, *27*, 1508-1530.

Hinz, K., Neben, S., Schreckenberger, B., Roeser, H. A., Block, M., De Souza, K. G., & Meyer, H. (1999). The Argentine continental margin north of 48 S: sedimentary successions, volcanic activity during breakup. *Marine and Petroleum Geology*, *16*(1), 1-25.

Isola, J. I., Bravo, M. E., Bozzano, G., Palma, F. I., Ormazabal, J. P., Principi, S., Spoltore, R. M., Martin, R., Esteban, F. D., & Tassone, A. A. (2021). The Late-Quaternary deposits of the Piedra Buena Terrace (Patagonian continental slope, SW Atlantic): An example of interaction between bottom currents and seafloor morphology. *Marine Geology*, *435*, 106459.

Ivanova, E. V., Borisov, D. G., Murdmaa, I. O., Belyaev, N. A., Zinger, T. F., Nemchenko, N. V., Simagin, N. V., Sipko, A. A., & Shulga, N. A. (2020).

Investigation of the Modern Lateral Sedimentation on the Argentine Continental Slope during Cruise 79 of the R/VAkademik Mstislav Keldysh. *Oceanology*, *60*(6), 869-871.

Lamy, F., Kilian, R., Arz, H. W., Francois, J. P., Kaiser, J., Prange, M., & Steinke, T. (2010). Holocene changes in the position and intensity of the southern westerly wind belt. *Nature Geoscience*, *3*(10), 695-699.

Lastras, G., Acosta, J., Muñoz, A., & Canals, M. (2011). Submarine canyon formation and evolution in the Argentine Continental Margin between 44 30'S and 48 S. *Geomorphology*, *128*(3-4), 116-136.

Mayr, C., Wille, M., Haberzettl, T., Fey, M., Janssen, S., Lücke, A., Ohlendort, C., Schabitz, O. G. Schlesr, G., & Zolitschka, B. (2007). Holocene variability of the Southern Hemisphere westerlies in Argentinean Patagonia (52 S). *Quaternary Science Reviews*, *26*(5-6), 579-584.

Miller, K. G., Kominz, M. A., Browning, J. V., Wright, J. D., Mountain, G. S., Katz, M. E., Sugarman, P. J., Cramer, B. S., Christie-Blick, N., & Pekar, S. F. (2005). The Phanerozoic record of global sea-level change. *science*, *310*(5752), 1293-1298.

Mortlock, R. A., Charles, C. D., Froelich, P. N., Zibello, M. A., Saltzman, J., Hays, J. D., & Burckle, L. H. (1991). Evidence for lower productivity in the Antarctic Ocean during the last glaciation. *Nature*, *351*(6323), 220-223.

Mortlock, R. A., & Froelich, P. N. (1989). A simple method for the rapid determination of biogenic opal in pelagic marine sediments. *Deep Sea Research Part A. Oceanographic Research Papers*, *36*(9), 1415-1426.

Munk, W. H., & Palmén, E. (1951). Note on the dynamics of the antarctic circumpolar current 1. *Tellus*, *3*(1), 53-55.

Murdmaa, I. O., Seitkalieva, E. A., Dara, O. M., Dorokhova, E. V., & Simagin, N. V. (2018). Glauconite sand from the terrace of the Patagonian continental slope, Southwestern Atlantic. *Lithology and Mineral Resources*, *53*(6), 455-459.

Piola, A. R., Matano, R. P., Steele, J. H., Thorpe, S. A., & Turekian, K. K. (2001). Brazil and Falklands (Malvinas) currents. *Ocean currents*, 35-43.

Preu, B., Schwenk, T., Hernández-Molina, F. J., Violante, R., Paterlini, M., Krastel, S., Tomasini, J., & Spieß, V. (2012). Sedimentary growth pattern on the northern Argentine slope: the impact of North Atlantic Deep Water on southern hemisphere slope architecture. *Marine Geology*, *329*, 113-125.

Reid, J. L. (1989). On the total geostrophic circulation of the South Atlantic Ocean: Flow patterns, tracers, and transports. *Progress in Oceanography*, *23*(3), 149-244.

Rintoul, S. R. (2000). Southern Ocean currents and climate. In *Papers and proceedings of the Royal Society of Tasmania* (Vol. 133, No. 3, pp. 41-50).

Ryan, W. B., Carbotte, S. M., Coplan, J. O., O'Hara, S., Melkonian, A., Arko, R., Weissel, R. A., Ferrini, V., Goodwillie, A., Nitsche, F., Bonczkowski, J., & Zemsky, R. (2009). Global multi-resolution topography synthesis. *Geochemistry, Geophysics, Geosystems*, *10*(3).

Taylor-Silva, B. I., & Riesselman, C. R. (2018). Polar frontal migration in the warm late Pliocene: Diatom evidence from the Wilkes Land margin, East

Antarctica. *Paleoceanography and Paleoclimatology*, *33*(1), 76-92. https://doi.org/10.1002/2017PA003225.

Toggweiler, J. R., Russell, J. L., & Carson, S. R. (2006). Midlatitude westerlies, atmospheric CO2, and climate change during the ice ages. *Paleoceanography*, *21*(2). doi:10.1029/2005PA001154.

Toggweiler, J. R. (2009). Shifting westerlies. *Science*, *323*(5920), 1434-1435. doi:10.1126/science.1169823.

Warratz, G., Henrich, R., Voigt, I., Chiessi, C. M., Kuhn, G., & Lantzsch, H. (2017). Deglacial changes in the strength of deep southern component water and sediment supply at the Argentine continental margin. *Paleoceanography*, *32*(8), 796-812.

Warratz, G., Schwenk, T., Voigt, I., Bozzano, G., Henrich, R., Violante, R., & Lantzsch, H. (2019). Interaction of a deep-sea current with a blind submarine canyon (Mar del Plata Canyon, Argentina). *Marine Geology*, *417*, 106002.

TABLES

Table 1			
Core	**Latitude**	**Longitude**	**Water Depth (m)**
58 JPC	-45.2638	-58.3298	2453
43 JPC	-45.6399	-58.5486	2350
32 JPC	-46.412	-58.3668	2490
29 JPC	-46.6383	-58.5943	2349
27 GC	-46.6382	-58.5945	2349
30 JPC	-46.6648	-58.6506	2309
57 JPC	-47.1673	-58.6148	2460
25 JPC	-47.8015	-58.0032	2612

Table 1: Coordinates and water depth of Piedra Buena cores.

Table 2: Lithostratigraphic Units in Core 27 GC		
Unit	**Interval (cm)**	**Lithology**
I	0-25	Foraminifera-rich Carbonate ooze
II	25-45	Quartz-glauconite sand
III	45-165	Foraminifera-rich Carbonate ooze with variable Glauconite and quartz
IV	165-255	Quartz-glauconite sand
V	255-355	Foraminiferal ooze

Table 2: Lithostratigraphic Unit description

Table 3			
Depth (cm)	**%Opal**	***N. pachy (s)* O18 PDB**	**% Coarse**
5	2.49	2.23	64.73
15	2.75	2.13	60.22
25			86.19
35	0.96		97.99
45		3.07	78.42
55		3.01	79.87
65	2.85	2.98	70.75
75	2.80	2.84	76.36
85		3.37	36.76
95		3.25	77.42
105	3.60	3.39	50.68
115	5.77	3.46	49.48
125		2.99	50.73
135	6.41	1.75	35.38
145		1.9	28.51
155		2.07	41.21
165	4.89	2.25	59.41
175	1.49		86.91
185			93.64
195	1.57		92.33
205			79.82
215	2.19		96.76
225			90.19
235	1.57		95.24
245	1.23		94.05
255		3.34	71.83
265		3.07	30.29
275	3.10	2.51	11.59
285		2.47	17.76
295		2.43	8.90
305		2.44	4.99
315		2.2	5.08
325	1.45	2.07	3.29
335		2.32	4.75
345	2.97	2.17	2.71
355		2.04	2.87

Table 3: Data of weight % Opal, planktonic $\delta^{18}O$, and coarse fraction.

27 GC Calculated Sedimentation Rates Based on Age Model						
LSU	**Core Depth (cm)**	**MIS**	**Approx. Age (kyr)**	**Thickness (cm)**	**Duration (kyr)**	**Rate (cm/kyr)**
I	**0-25**	**1 to 2**	**0 to 12**	25	12	**2.08**
II	**25-45**	**2 to 3**	**12 to 35**	20	23	**0.87**
III	**45-170**	**3 to 6a**	**35 to 135**	125	100	**1.25**
IV	**170-255**	**6a to 7a**	**135 to 190**	85	55	**1.55**
V	**255-355**	**7a to 7d**	**190 to 220**	100	30	**3.33**

Table 4. Sedimentation Rates of Lithostratigraphic Units Based on Age Model. Age model I (AMI) and Age model II (AMII) are based on lithostratigraphic units (LSU), core depth, and age assignment duration. AMI interprets LSU IV as MIS-5b through MIS-5d and LSU V as MIS-5e. AMII interprets LSU IV as MIS-6a through MIS-6e and LSU V as MIS-7. Rates were calculated based on LSU thickness and differences in age duration of interpreted MIS. AMI shows higher sedimentation rates in LSU IV and V while AMII shows lower sedimentation rates in LSU IV and V.

FIGURES

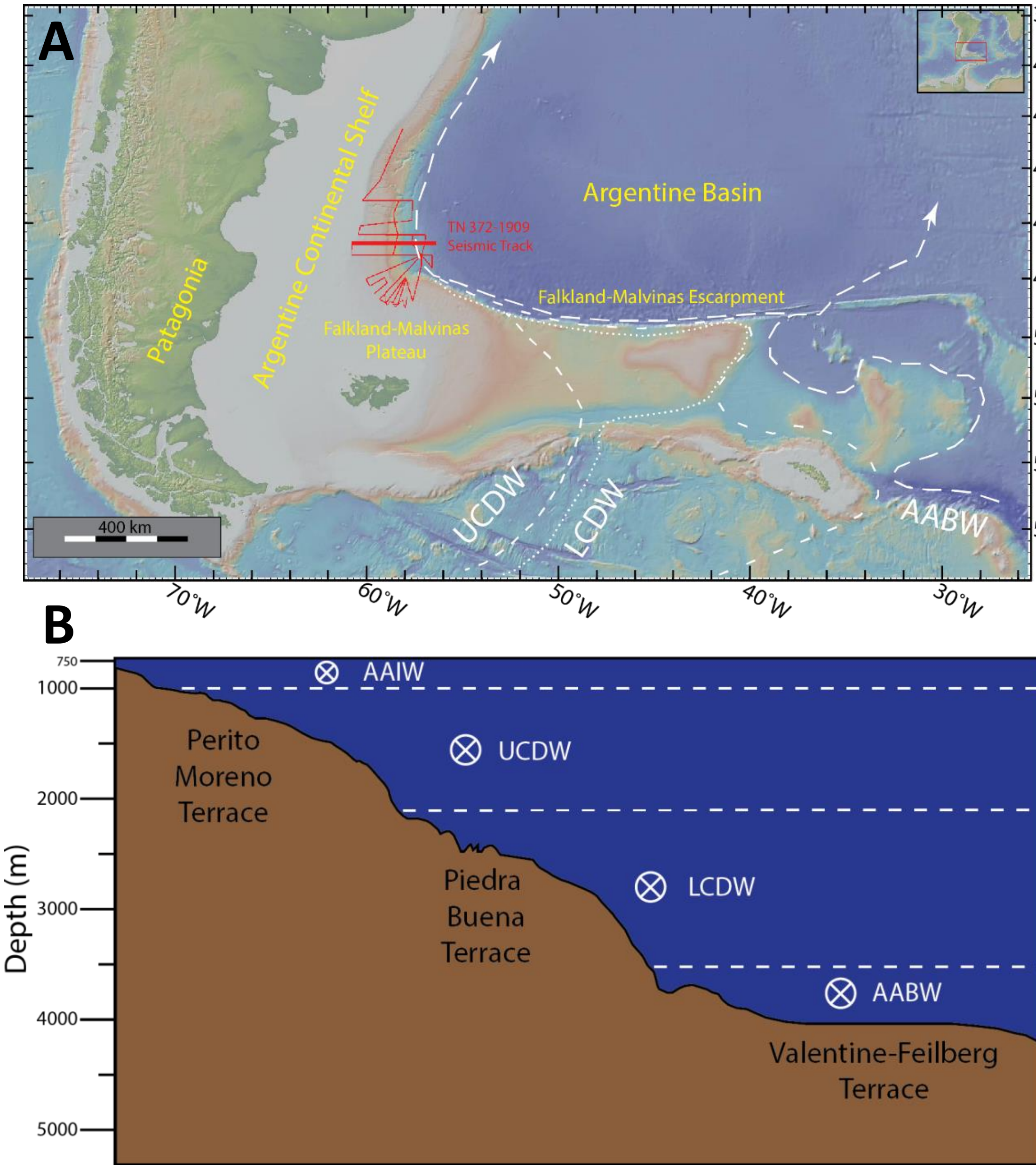

Figure 1. Overview of the Argentine margin. A) Overview of the Argentine margin showing Southern Ocean sourced water masses flowing into the Argentine Basin. T he various dashed white lines represent individual flow paths. The red lines along the Argentine Continental Shelf north of the Falkland-Malvinas Island represent the seismic lines from the TN 372-1909 cruise. The bold red line represents seismic line 37 used create bathymetric profile seen in Figure 1B. B) Three of the four terraces pictured: Nagera, Perito Moreno, Piedra Buena, and Valentin-Feilberg with the interacting water masses. Modified after Gruetzner et al., 2011. Figure made with GeoMapApp (www.geomapapp.org) / CC BY / CC BY (Ryan et al., 2009).

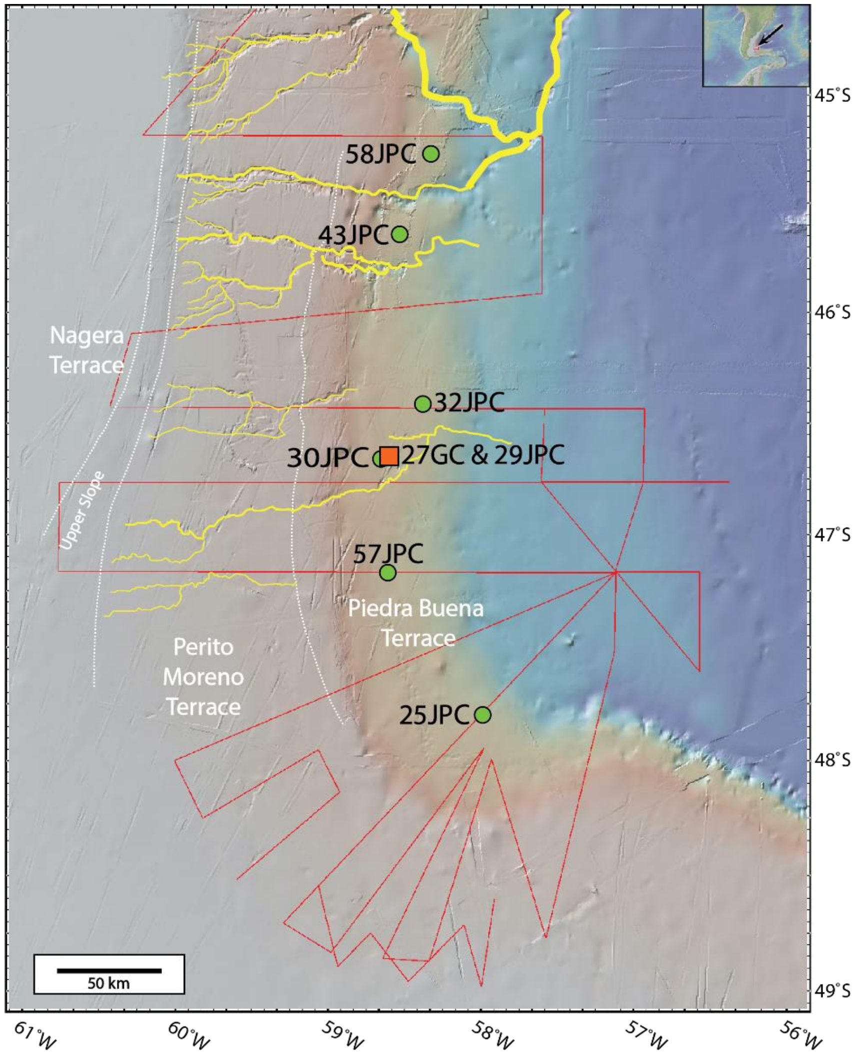

Figure 2. Map of field site. A) The orange square indicates the location of core 27 GC. The green circles indicate the locations of the Piedra Buena JPCs. The red lines indicate ship tracks of seismic survey. White-dotted lines indicate boundaries of different oceanographic provinces along the margin. Modified from Lastras et al., (2011). Yellow lines represent canyon systems also modified from Lastras et al., (2011). Figure made with GeoMapApp (www.geomapapp.org) / CC BY / CC BY (Ryan et al., 2009). B) 3.5 kHz image of 27 GC coring site.

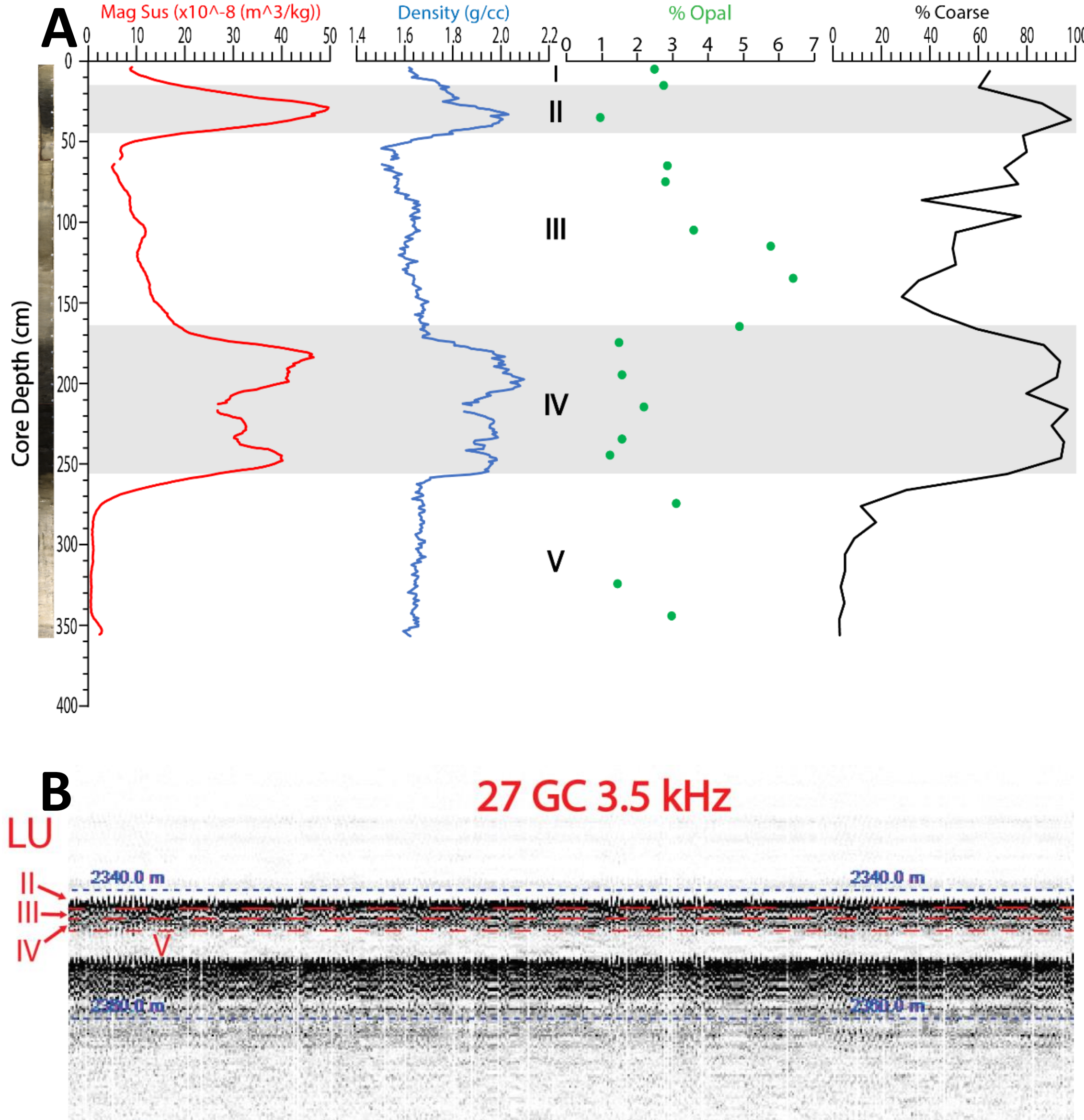

Figure 3. Compiled results of 27 GC analysis. (A) Red curve represents magnetic susceptibility, blue curve represents density, green curve represents weight % opal, black curve represents the coarse fraction. Gray shading added to enhance figure readability. Based on these results lithostratigraphic units I-V were established. To the right, a scaled color scan of the core photograph. (B) 3.5kHz of 27GC coring location with labelled lithostratigraphic units to the right. Lithostratigraphic unit I is not visible, but units II-V are visible.

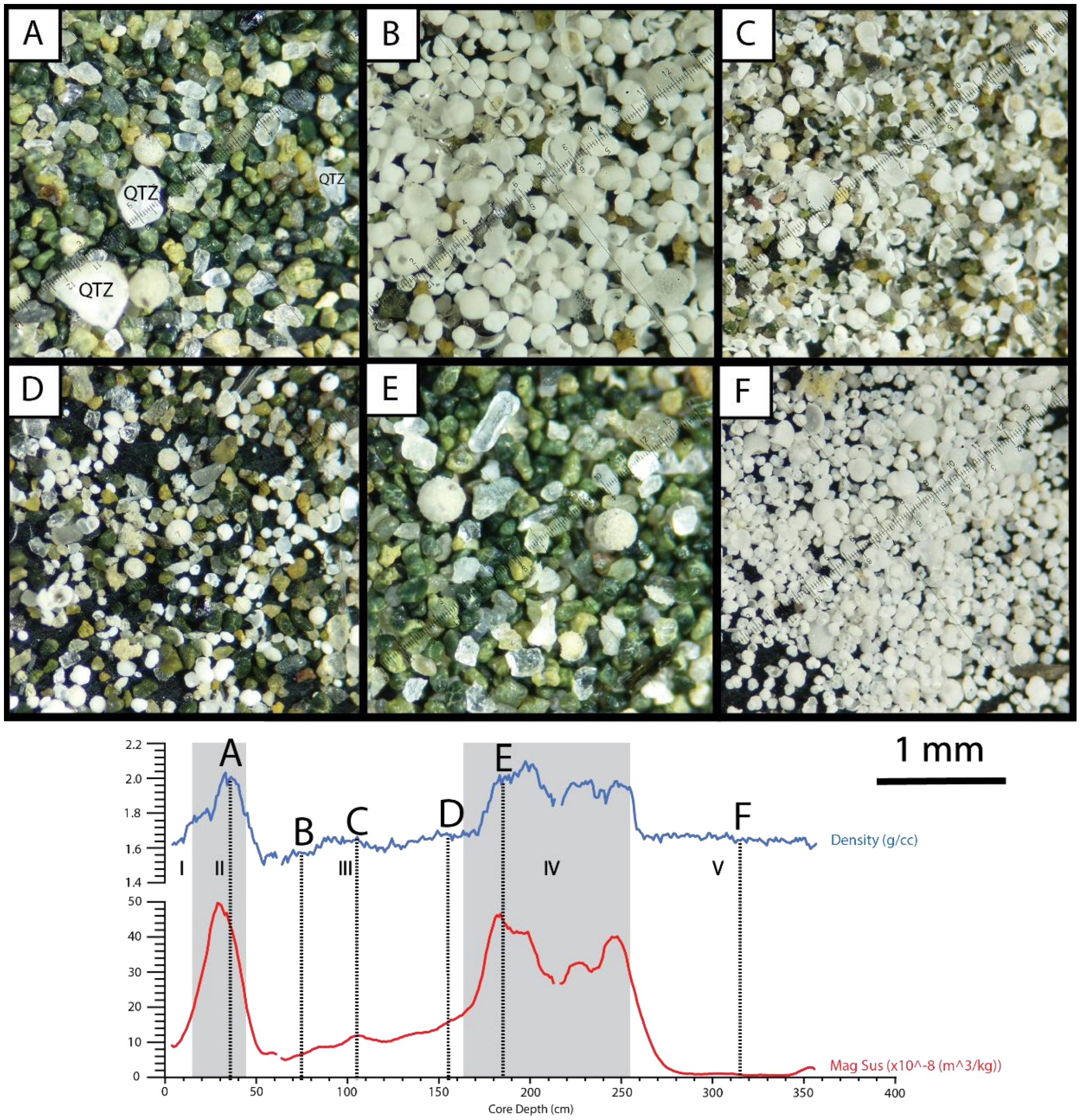

Figure 4. Sample composition compared with core logger data of 27 GC. Dashed black lines indicate the depth of the associated sediment sample. Gray shading added to enhance figure readability. Sample 35-37cm (A) consists of coarse quartz sand grains mixed with glauconite sand. 75-77 cm (B) consists of mostly foraminifera, with glauconite grains in low abundance. 105-107 cm (C) taken from a slightly higher magnetic susceptibility and density peak, shows an increased abundance of glauconite, appearing nearly equal to the foraminifera component. 165-167 cm (D) falls on an area that is rapidly increasing in magnetic susceptibility and density. This sample shows an increased abundance of glauconite which has a larger component than the foraminifera. 185-187 cm (E) taken from the most pronounced dark unit in the entire core associated with the first sub unit within lithostratigraphic unit IV315-317 cm (F) is correlated with the lowest core logger values, sediments are nearly all foraminiferal remains with the occasional quartz or glauconite grain interspersed throughout.

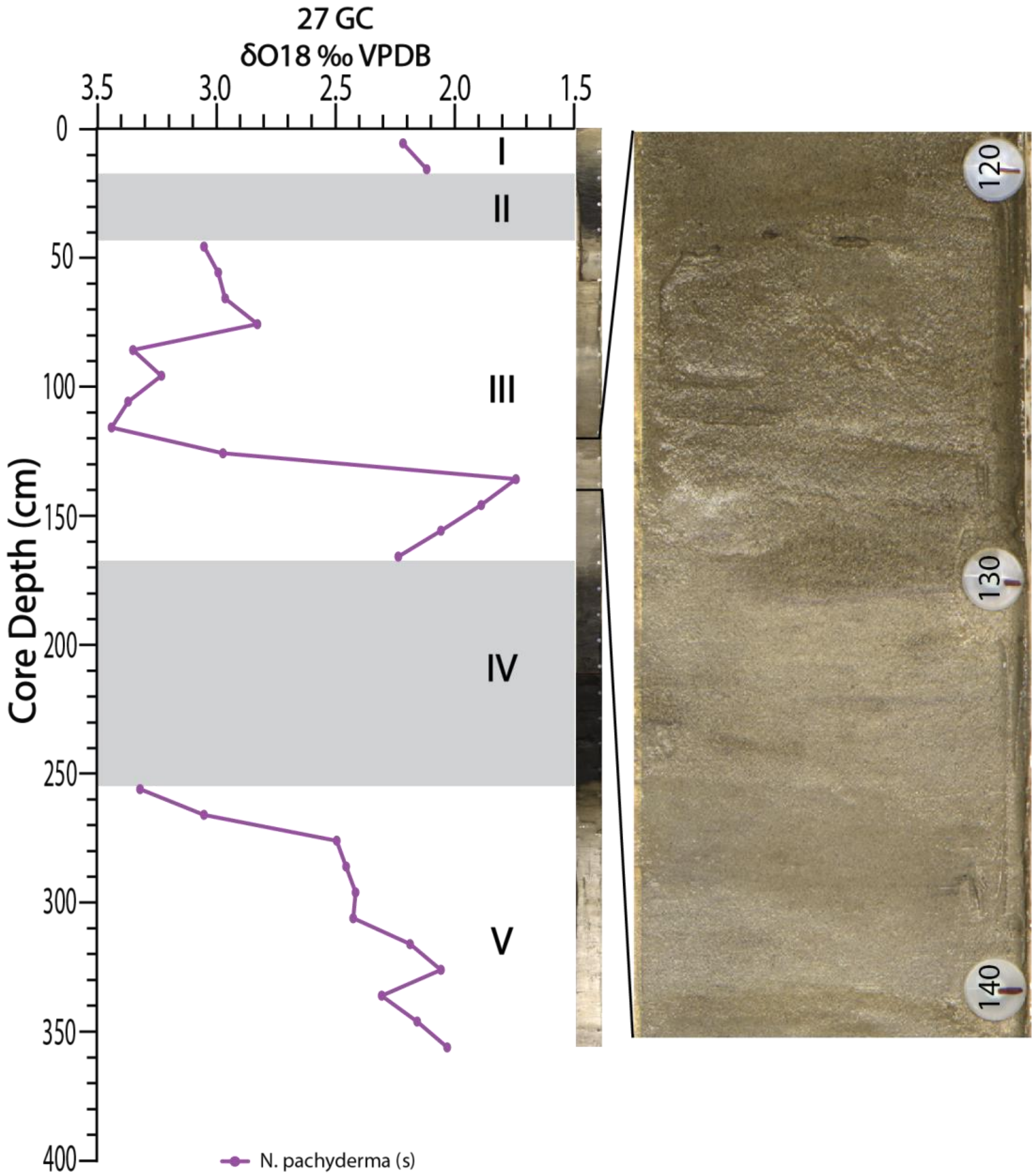

Figure 5. δ^{18}O of planktonic foraminifera. *N. pachyderma* (s) δ^{18}O in Lithostratigraphic units I, III, and V. Lithostratigraphic units II and IV was composed of quartz-glauconite sands with no foraminifera. Gray shading added to enhance figure readability. Note the increasing δ^{18}O values from unit III before foraminifera disappear in unit IV and the decreasing values from the IV-V transition into V. This suggests climate began cooling and sea level was falling in unit III and unit IV was deposited during a glacial period. At the top of unit V, values are low and increasing suggesting climate was in a glacial during unit IV and transitioned to an interglacial in unit V.

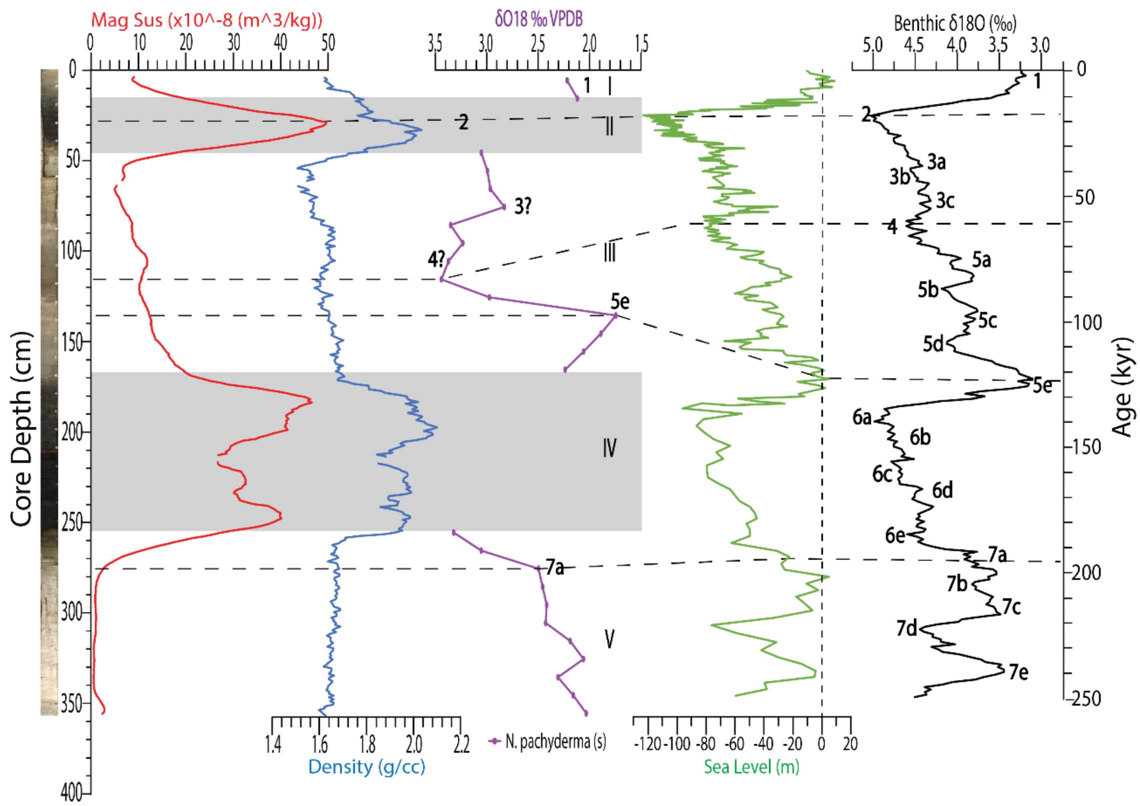

Figure 6. Age Model. Red curve represents magnetic susceptibility, blue curve represents density, purple curve represents $\delta^{18}O$ of *N. pachyderma* (s), green curve represents the Miller et al, (2005) sea level curve, and the black curve represents the Lisiecki and Raymo, (2005) benthic stacked record. Gray shading added to enhance figure readability. Intervals of glauconite are associated with glacial periods, while the intervals of carbonate ooze are associated with interglacial periods. Based on this hypothesis, MIS were assigned at different depths of the core. It is interpreted that LU I is MIS-1, LU II is MIS-2. The top of LU III may be MIS-3 and the lowest $\delta^{18}O$ value (135 cm) is interpreted as MIS-5e. LU IV is interpreted as MIS-6a through MIS-6e and LSU V as MIS-7. Alternate age models can be created, but constraining them will require additional $\delta^{18}O$ of planktonic foraminifera data and identification of additional biostratigraphic markers.

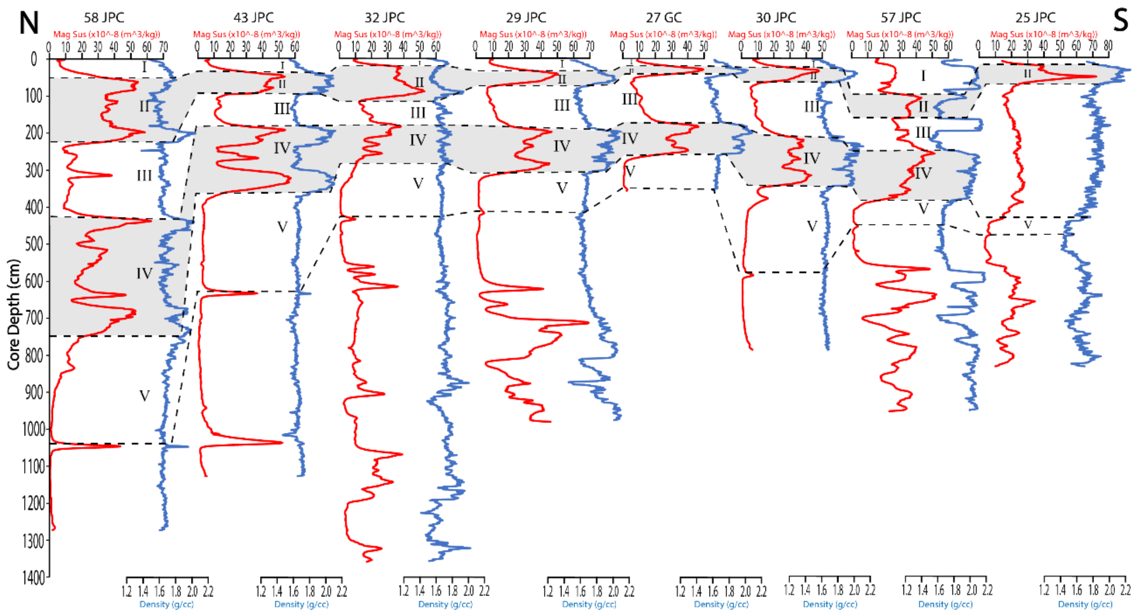

Figure 7. Piedra Buena Correlation. Red curves represent magnetic susceptibility. Blue curves represent density. Dashed black lines indicate predicted lines of facies boundary correlation. Gray shading added to enhance figure readability. Each correlated unit was labelled based on the unit identification based on 27 GC. In general, cores north of 27 GC showed greater sedimentation with expanded sections while cores south of 27 GC show either missing or compacted sections.

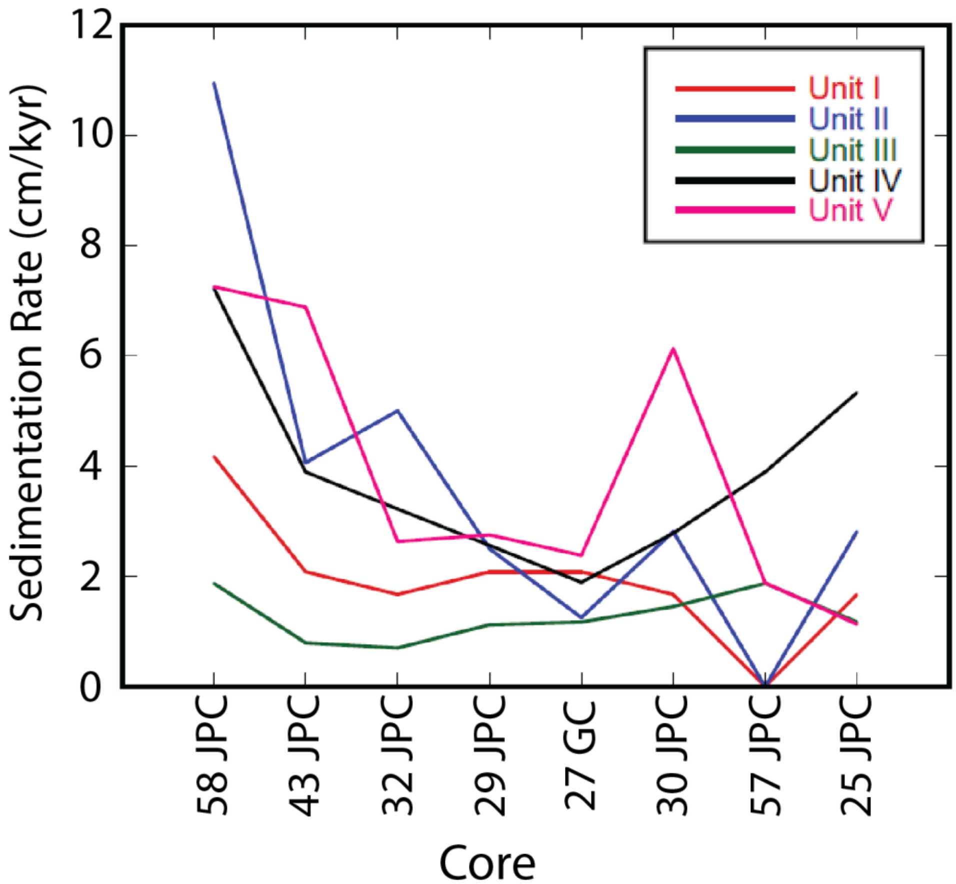

Figure 8. Core Sedimentation Rates based on age model. Cores to the left are more north along the Piedra Buena terrace while cores to the right are further south. The general trend shows cores to the north exhibit thicker lithostratigraphic unit thicknesses thus higher sedimentation rates.

APPENDIX

Appendix 1									
Depth (cm)	Density (g/cc)	MS (x 10^-8 (m^3/kg))	%Opal	*N. pachy (s)* C13 PDB	*N. pachy (s)* O18 PDB	*N. pachy (d)* C13 PDB	*N. pachy (d)* O18 PDB	*G. bulloides* C13 PDB	*G. bulloides* O18 PDB
5	1.63	9.49	2.49	0.76	2.23			0.83	2.45
15	1.75	22.38	2.75	0.53	2.13			0.57	2.72
25	1.83	46.75							
35	1.99	41.80	0.96						
45	1.71	15.12		0.72	3.07	0.99	2.69	0.55	3.22
55	1.56	6.87		0.54	3.01			-0.18	2.78
65	1.52	5.11	2.85	0.71	2.98			0.45	3.32
75	1.57	6.89	2.80	0.55	2.84	0.59	2.59	0.22	3.39
85	1.66	8.59		0.9	3.37			0.63	3.18
95	1.66	9.43		0.83	3.25	0.86	2.96	0.56	3.01
105	1.64	11.82	3.60	0.48	3.39				
115	1.60	10.45	5.77	1.09	3.46			0.86	2.92
125	1.62	10.88		0.81	2.99			0.69	2.51
135	1.64	12.51	6.41	0.07	1.75	0.50	1.66	0.13	2.34
145	1.66	13.34		0.16	1.9	0.26	1.76	0.18	2.24
155	1.64	16.41		0.17	2.07			0.10	2.39
165	1.69	19.83	4.89	-0.35	2.25	0.10	1.81	-0.27	2.46
175	1.86	37.27	1.49						
185	1.99	43.57							
195	2.10	40.96	1.57						
205	1.96	30.19							
215	1.85	26.78	2.19						
225	1.95	32.72							
235	1.89	31.30	1.57						
245	1.98	39.91	1.23						
255	1.77	25.49		0.93	3.34	1.07	2.25	0.68	2.69
265	1.65	9.14		1.18	3.07	1.29	2.24	1.01	2.82
275	1.66	2.27	3.10	1.14	2.51			0.95	2.56
285	1.67	1.03		1.22	2.47			0.65	2.60
295	1.68	0.91		1.13	2.43			0.20	2.07
305	1.69	0.98		1.04	2.44			1.00	2.70
315	1.65	0.65		0.93	2.2			0.74	2.53
325	1.64	0.70	1.45	0.94	2.07			0.45	2.67
335	1.65	0.57		1.05	2.32			0.52	2.25
345	1.66	1.52	2.97	0.93	2.17				
355	1.62	2.37		0.62	2.04				

Appendix 1: MSCL, Weight % Opal, and Planktonic $\delta^{13}C$ and $\delta^{18}O$ data

Appendix 2: Point Counts									
Component	**5-7 cm***	**35-37 cm**	**75-77 cm**	**105-107 cm**	**165-167 cm**	**185-187 cm**	**225-227 cm**	**245-247 cm**	**315-317 cm**
	%	**%**	**%**	**%**	**%**	**%**	**%**	**%**	**%**
Glauconite	23.49	46.67	15	19.66	43.66	58.33	46	52	0.66
Quartz	12.69	36	4	10	19.66	32.33	38	30.66	1.66
Radiolarian	2.22	7.66	10	15	2	3	7.33	10.33	1.33
Adamantine Black	0.317	1	0	0.33	0.66	0.66	1	1	0
Gray Metallic	6.03	8	1	1.33	5.6	5.33	6	6	0.66
Spicules	1.58	0.33	1	0.66	0.66	0	1	0	0.66
Foraminifera	53.637	0	65.33	51.95	25.98	0	0	0	93.9
Diatom	0	0	3.66	1	1.66	0.33	0.66	0	1

*Point count used 315 grains.

Appendix 2: Point count results.

Correlated Lithstratigraphic Unit Sedimentation Rates							
Core ID	**LSU**	**Core Depth (cm)**	**Thickness (cm)**	**MIC**	**Approx. Age (kyr)**	**Duration (kyr)**	**Rate (cm/kyr)**
58 JPC	**I**	**0-50**	50	1 to 2	0 to 12	12	**4.17**
	II	**50-225**	175	2 to 3	12 to 35	23	**7.61**
	III	**225-425**	200	3 to 6a	35 to 135	100	**2.00**
	IV	**425-750**	325	6a to 7a	135 to 190	55	**5.91**
	V	**750-1040**	290	7a to 7d	190 to 220	30	**9.67**
43 JPC	**I**	**0-25**	25	1 to 2	0 to 12	12	**2.08**
	II	**25-90**	65	2 to 3	12 to 35	23	**2.83**
	III	**90-175**	85	3 to 6a	35 to 135	100	**0.85**
	IV	**175-350**	175	6a to 7a	135 to 190	55	**3.18**
	V	**350-625**	275	7a to 7d	190 to 220	30	**9.17**
32 JPC	**I**	**0-20**	20	1 to 2	0 to 12	12	**1.67**
	II	**20-100**	80	2 to 3	12 to 35	23	**3.48**
	III	**100-175**	75	3 to 6a	35 to 135	100	**0.75**
	IV	**175-320**	145	6a to 7a	135 to 190	55	**2.64**
	V	**320-425**	105	7a to 7d	190 to 220	30	**3.50**
29 JPC	**I**	**0-25**	25	1 to 2	0 to 12	12	**2.08**
	II	**25-65**	40	2 to 3	12 to 35	23	**1.74**
	III	**65-185**	120	3 to 6a	35 to 135	100	**1.20**
	IV	**185-300**	115	6a to 7a	135 to 190	55	**2.09**
	V	**300-410**	110	7a to 7d	190 to 220	30	**3.67**
27 JPC	**I**	**0-25**	25	1 to 2	0 to 12	12	**2.08**
	II	**25-45**	20	2 to 3	12 to 35	23	**0.87**
	III	**45-170**	125	3 to 6a	35 to 135	100	**1.25**
	IV	**170-255**	85	6a to 7a	135 to 190	55	**1.55**
	V	**255-350**	95	7a to 7d	190 to 220	30	**3.17**
30JPC	**I**	**0-20**	20	1 to 2	0 to 12	12	**1.67**
	II	**20-65**	45	2 to 3	12 to 35	23	**1.96**
	III	**65-220**	155	3 to 6a	35 to 135	100	**1.55**
	IV	**220-345**	125	6a to 7a	135 to 190	55	**2.27**
	V	**345-590**	245	7a to 7d	190 to 220	30	**8.17**
57 JPC	**I**	**0-100**	100	1 to 2	0 to 12	12	**8.33**
	II	**100-160**	60	2 to 3	12 to 35	23	**2.61**
	III	**160-250**	90	3 to 6a	35 to 135	100	**0.90**
	IV	**250-375**	125	6a to 7a	135 to 190	55	**2.27**
	V	**375-450**	75	7a to 7d	190 to 220	30	**2.50**
25 JPC	**I**	**0-20**	20	1 to 2	0 to 12	12	**1.67**
	II	**20-65**	45	2 to 3	12 to 35	23	**1.96**
	III	**N/A**	N/A	3 to 6a	35 to 135	100	**N/A**
	IV	**430**	N/A	6a to 7a	135 to 190	55	**N/A**
	V	**430-475**	45	7a to 7d	190 to 220	30	**1.50**

Appendix 3: Lithostratigraphic unit sedimentation rates based on correlation. Top of the table represents cores taken further to the north, the bottom of the table represents cores taken to the south. Calculated sedimentation rates of all Piedra Buena cores were based on lithostratigraphic unit thicknesses with approximate ages of MIC based on the age model presented in this thesis.